Polymeric carbon nitride-based photocathodes for visible light-driven selective reduction of oxygen to hydrogen peroxide

Hanna Braun[a], Dariusz Mitoraj[a], Joanna Kuncewicz[b], Andreas Hellmann[c], Mohamed M. Elnagar[a], Joachim Bansmann[d], Christine Kranz[c], Timo Jacob[a], Wojciech Macyk[b], Radim Beranek[a*]

[a] Institute of Electrochemistry, Ulm University, Albert-Einstein-Allee 47, 89081 Ulm, Germany

[b] Faculty of Chemistry, Jagiellonian University, ul. Gronostajowa 2, 30-387 Kraków, Poland

[c] Institute of Analytical and Bioanalytical Chemistry, Ulm University, Albert-Einstein-Allee 11, 89081 Ulm, Germany

[d] Institute of Surface Chemistry and Catalysis, Ulm University, Albert-Einstein-Allee 47, 89081 Ulm, Germany

*Corresponding author: radim.beranek@uni-ulm.de

This article is an appreciation of the contributions to the field of photocatalysis made by Professor Detlef Bahnemann

Abstract

Polymeric carbon nitrides (PCN) are sustainable, tunable, non-toxic and chemically stable materials that represent highly promising heterogeneous photocatalysts for light-driven hydrogen peroxide production *via* selective reduction of dioxygen. However, most of the studies on photocatalytic H_2O_2 production using PCN-based photocatalysts reported so far have used PCN powder suspensions and have been carried out in the presence of additional (sacrificial) electron donors, such as aliphatic or aromatic alcohols. Herein, we report the first multicomponent hybrid photocathode based on PCN that is capable of selective reduction of dioxygen to H_2O_2 under visible light irradiation (420 nm LED). A comparative analysis of various photocathode architectures is carried out using electronic absorption spectroscopy, surface photovoltage spectroscopy, open-circuit photopotential spectroscopy, and photocurrent measurements, including *in-situ* detection of formed H_2O_2 using microelectrodes. Notably, the ability of PCN-based photocathodes to catalyze the light-driven reduction of O_2 to H_2O_2 in the absence of any additional electron donor is unambiguously demonstrated. Our study thus highlights the intrinsic nature of the photocatalytic activity of PCN in H_2O_2 production, and paves the way for the development of further PCN-based photocathodes in which PCN could be coupled with more effective light absorbers to increase the overall performance.

Graphical abstract

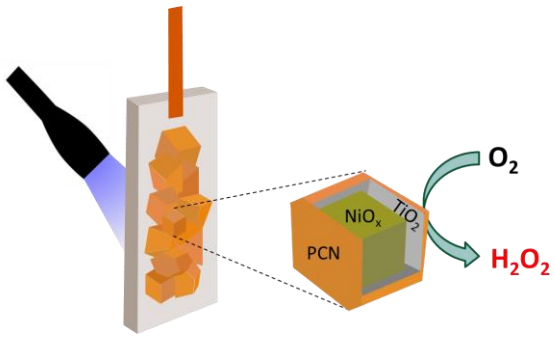

Keywords: Photoelectrochemistry, Photocatalysis, Selectivity, Carbon nitride, Oxygen activation

1. Introduction

Polymeric carbon nitrides (PCN) are sustainable, tunable, non-toxic and chemically stable materials,[1-4] that have been utilized in the construction of various photocatalytic systems for a wide range of light-driven reactions, including hydrogen evolution,[5-10] water oxidation,[6, 11, 12] CO_2 reduction,[13, 14] organic pollutant degradation,[15-17] or selective chemical conversions [18-21]. Notably, a vast majority of the studies on PCN-based photocatalytic systems encompassed investigations of *suspensions* of PCN powders, whereas studies of *photoelectrocatalytic* systems utilizing PCN-based *photoelectrodes* are much less frequent. In this context, it is important to realize that – apart from some drawbacks (*e.g.*, increased installation costs due to photoelectrode and reactor fabrication) – there are several advantages associated with carrying out photoelectrocatalytic reactions in well-designed photoelectrochemical cells. From a technological point of view, it is preferable to have the products of the oxidation and reduction reactions separated in the two compartments of the photoelectrochemical cell. Furthermore, the (photo)anodic and (photo)cathodic half-cells can be first optimized separately, to be – eventually – implemented into a tandem photoelectrochemical device. Finally, from a more fundamental and scientific point of view, photoelectrocatalytic cells allow for studying light-driven conversions also in the *absence* of any additional (sacrificial) oxidizing and reducing agents which are typically used in photocatalytic studies using suspensions. Indeed, it is one of the many significant scientific contributions of Professor Detlef Bahnemann that he has repeatedly pointed out how the activity of many photocatalytic systems is often dictated by the reactivity of the sacrificial reagents, rather than by the intrinsic charge-separation dynamics and kinetics of photocatalyzed redox reactions under investigation [22, 23]. Studies of truly photoelectrocatalytic systems without any additional reducing and oxidizing agents are therefore of paramount importance.

However, the fabrication of PCN-based photoelectrodes is rather challenging, mainly due to poor adhesion of PCN to conductive substrates [24-27] and low conductivity of PCN that hinders the transport of photogenerated charge carriers into the external circuit [28]. The development of effective PCN-based *photoanodes* has been enabled mainly by two approaches. Either conventional [26, 27] or ionic carbon nitride [29, 30] films were directly deposited onto conductive substrates, or PCN was deposited onto porous metal oxide (*e.g.*, TiO_2 or ITO) films acting as a scaffold and an effective *n*-type electron collector [11, 12, 31-36]. In a similar vein, PCN-based photocathodes have been fabricated either as pristine [37] or biopolymer-activated films,[38] or in combination with *p*-type semiconductors (*e.g.*, $CuGaSe_2$ [39], CuI [40] or NiO [41, 42]) acting as effective hole collectors.

One of the most attractive reductive conversions that is rather effectively photocatalyzed by PCN materials is the two-electron reduction of dioxygen to hydrogen peroxide [43]. H_2O_2 represents a highly valuable commodity chemical that is being used as a versatile and environmentally benign oxidizing agent in a number of important industrial processes. Although photocatalytic H_2O_2 production at PCN from pure water and oxygen has been reported,[44] typically the presence of additional sacrificial electron donors (*e.g.*, aliphatic or aromatic alcohols) is practically indispensable in order to achieve reasonable reaction rates [18, 21, 44-47]. The key mechanistic steps proposed in the literature are the protonation of the heptazine nitrogen sites enabled by fast oxidation of the electron donor [48] and the activation of O_2 by photogenerated electrons, enabled by the very negative *quasi*-Fermi level of electrons in PCN (typically ca. –0.7 V *vs*. RHE [34]), with subsequent formation of the intermediate heptazine-bound endoperoxide species [18, 44]. While photocathodes for efficient H_2O_2 production from O_2 based, for example, on epindolidione deposited on gold electrodes [49] or porphyrin-sensitized nickel oxide films [50] have been reported recently, there are – to the best of our knowledge – no PCN-based photocathodes for selective light-driven reduction of O_2 to H_2O_2 reported so far.

Herein, we report for the first time a multicomponent hybrid photocathode based on PCN for selective reduction of O_2 to H_2O_2 under visible light irradiation (420 nm LED), whereby the desired H_2O_2 product is determined *in-situ* using microelectrodes. The optimized photocathode architecture comprises PCN deposited on a porous NiO_x film acting as a scaffold for effective extraction and collection of photogenerated holes. A detailed analysis of various photoelectrode configurations shows that the presence of PCN is crucial for obtaining H_2O_2 as a product, and provides evidence for the beneficial effect of a TiO_2 interlayer on the overall photoelectrocatalytic performance.

2. Experimental

2.1 Materials

Fluorine-doped tin oxide (FTO) Pilkington TEC glass was purchased from the XOP company (XOP Glass, Castellón Spain). For rinsing deionized water was used. For the preparation of the electrodes nickel(II) chloride hexahydrate ($NiCl_2 \cdot 6\,H_2O$, 99.9%) and titanium tetraisopropoxide were purchased from Sigma Aldrich as well as 2-propanol, ethanol (99.95%) from VWR Chemicals and polyethylene glycol (PEG) 10000 from Alfa Aesar. Urea, boric acid (99.8%) and hydrochloric acid (37%) were provided by Merck.

2.2 Photocathode preparation

The NiO_x films were fabricated using a modified method reported by Sun *et al.* [51]. A mixture of 2.74 g of $NiCl_2$, 1.5 g of deionized water, 1.5 g of ethanol and 0.5 g of PEG 10,000 was stirred for 24 h. The ratio was selected to obtain a 44 wt% content of $NiCl_2$. The films were deposited onto FTO glasses by dip coating for 10 min with a withdrawal speed of 25 mm s^{-1}. After drying in air, the electrodes were calcined at 450 °C for 30 min with a heating ramp of 15 °C min^{-1}. After cooling to room temperature, the second layer of NiO_x was deposited in the same way.

A TiO_2 layer was deposited on the electrode covered with NiO_x using dip-coating. For the preparation of the TiO_2 precursor solution, 15 mL of titanium tetraisopropoxide (TTIP) was slowly dropped into the solution of 0.4 mL of concentrated HCl mixed with 170 of mL isopropanol. To get a thin layer the withdrawal speed was 8 mm s^{-1}. Afterward, the electrode was dried for 1 h in air and calcined at 450 °C for 30 min with a heating ramp of 15 °C min^{-1}.

The PCN layer was prepared by placing the electrode in a Schlenk tube connected with a round bottom flask containing 1 g of urea and heated in a muffle oven for 30 min at 425 °C [33].

For comparative analyses, sets of electrodes covered with (i) NiO_x; (ii) NiO_x-PCN; (iii) NiO_x-TiO_2 and (iv) NiO_x-TiO_2-PCN were prepared at least in triplicate, and representative average data are reported.

2.3 Characterization methods

For the analysis of electronic absorption properties, a UV-Vis spectrometer (UV-2600, Shimadzu, Japan) equipped with an integrating sphere was used. The absorptance (Abs.) was calculated using the equation:

$$\text{Absorptance (\%)} = 100\% - \text{Reflectance (\%)} - \text{Transmittance (\%)} \quad (1)$$

For the determination of the bandgap using the Tauc formalism, the layers on the electrodes were scratched off and the diffuse reflectance of the powder diluted with barium sulfate as a reference was measured [52].

The morphology and elemental composition of the prepared layers were initially determined using a Vega 3 LM (Tescan) scanning electron microscope (SEM) equipped with a LaB_6 cathode and EDS detector (10 mm^2 *x*-act SDD detector, Oxford Instruments) operating at a primary voltage of 20 kV. Elemental composition is given in atomic percentages. In addition,

the cross-sections, chemical composition, and elemental mappings of the photocathodes were analyzed using a ZEISS LEO 1550 VP scanning electron microscope (SEM) operating at an acceleration voltage of 15 kV, coupled with energy dispersive spectroscopy (EDS, Ametek, USA).

The crystalline structure of the synthesized materials was studied using a MiniFlex 600 (Rigaku) X-ray diffractometer equipped with a CuK_{α} nickel-filtered source lamp (λ = 1.54 Å) operating at 40 kV voltage.

A commercial XPS instrument from Physical Electronics (PHI 5800 ESCA) equipped with a hemispherical electron analyzer, a monochromatic Al K_{α} X-ray source (1486.6 eV) and a flood gun to avoid charging of the sample was used for the measurements. Survey spectra were recorded using a pass energy of 93.9 eV, detail spectra with 29.35 eV. Both angles (angle of photon incidence on the sample and angle of emitted photoelectrons) are 45° with respect to the surface normal (sample holder, respectively). The binding energies (BEs) of all spectra were calibrated with respect to the C 1s peak of ubiquitous carbon, which was fixed at a binding energy (BE) of 284.8 eV. The data were evaluated (deconvolution of spectra) by using the commercial software package CasaXPS (Casa Software Ltd., version 2.3.23PR1.0). In a first step, a Shirley background subtraction was performed. The fitting of the Ti 2p spectra was performed according to data reported by Biesinger *et al*. [53] and Saari *et al.* [54].
Surface photovoltage (SPV) measurements were performed with a Kelvin probe (Instytut Fotonowy) combined with a monochromator and a Xenon arc lamp (Instytut Fotonowy). An oscillating reference electrode made of a gold grid was used. The electrodes were contacted using copper tape. First, the contact potential difference (CPD) in the dark was measured over time to stabilize the sample. The SPV measurements were carried out under ambient conditions under intermittent monochromatic irradiation (320 s / 60 data points in the dark, 320 s / 60 data points under illumination) from 500 nm to 300 nm with a step of 20 nm.

For the photoelectrochemical measurements, a standard three-electrode setup with a platinum wire as a counter electrode, an Ag/AgCl (3.5 M KCl, 0.207 V vs. SHE) reference electrode, and the prepared photocathodes as working electrodes with an irradiation area of 0.5 cm^2 was used. The Incident Photon-to-Current Efficiency (IPCE) and the Open Circuit Potential (OCP) *vs*. wavelength measurements were performed using a photoelectric spectrometer (Instytut Fotonowy) equipped with a Xenon lamp (150 W). The light was turned on and off every 5 s for the IPCE and OCP measurements. The determined IPCE values and the differential OCP were plotted against the wavelength.

For the Linear Sweep Voltammetry (LSV) measurements, an SP-300 potentiostat (BioLogic) and a 150 W Xe lamp (L.O.T.-Oriel) equipped with a KG3 heat filter and an AM1.5G filter with a light power density adjusted to ca. 100 mW cm^{-2} (1 sun) were used. Borate buffer (pH 9) was determined as the optimum electrolyte for all measurements. During the measurements, the solution was gently purged with molecular oxygen acting as an electron scavenger. Unless otherwise indicated, all electrodes were irradiated from the backside.

2.4 H_2O_2 detection

H_2O_2 detection was carried out using Prussian blue (PB)-modified Pt microelectrodes. Electrochemical deposition of PB on Pt microelectrodes (diam. 25 µm) was carried out according to previously published procedures [55-57]. In brief, four cycles in a potential range of 0.4 and 0.75 V *vs*. Ag/AgCl at a scan rate of 0.02 V/s were applied in a freshly prepared solution of 1.25 mM $K_3[Fe(CN)_6]$ and 1.25 mM $FeCl_3$ in 0.1 M HCl / 0.1 M KCl solution. After the deposition of PB, electrodes were rinsed with ultrapure water and activated by applying another 10 cycles in the electrolyte solution (0.1 M KCl / 0.1 M HCl). Finally, the electrodes were again rinsed with ultrapure water and then tempered at 80 °C for 1 h. *In-situ* H_2O_2 measurements were performed in a four-electrode setup (*i.e.*, using two working electrodes, WE1 and WE2) by positioning a PB-modified Pt microelectrode (diam. 25 µm, biased at –0.05 V *vs*. Ag/AgCl, WE1) at a distance of approx. 50 µm above the photocathode (biased at –0.8 V *vs*. Ag/AgCl, WE2) using a stepper motor and the help of an inverted microscope. The photocathode samples were illuminated with monochromatic light (420 nm LED) for 10 min in a 1.5 mL phosphate buffer solution (50 mM, pH 7). For measurements in oxygen-free conditions, the solution was purged 5 min prior with argon and a constant argon stream was kept over the measurement cell during the entire experiment. An optical fiber (diam. 1000 µm, M59-L01, Thorlabs GmbH, Bergkirchen, Germany) connected to a 110 mW blue LED (420 nm, M420F3, Thorlabs GmbH) was used for the illumination of the samples.

3. Results and Discussion

In order to fabricate mechanically stable PCN-based photocathodes, we used porous NiO_x films on FTO as a scaffold for subsequent deposition of PCN using chemical vapor deposition from urea decomposition products [33]. Nickel oxide is well established as a large bandgap (~3.3 eV) *p*-type semiconductor that can be used as a hole collector and/or hole transport layer in dye-sensitized photoelectrochemical cells [50, 51, 58, 59]. Since the intrinsic conductivity of PCN is typically very low [33], we envisaged that NiO_x should effectively extract holes from PCN

and transport them into the FTO substrate, enhancing thus the charge separation in our photocathodes. The top-view SEM images show that the NiO_x layer consists of polydispersed particles of an average diameter of ca. 120 nm (**Figs. 1a** and **e**). The NiO_x particles aggregate to form a porous network (**Fig. 1a**), and build a fiber-like structure after modification with TiO_2 and/or PCN (**Fig. 1b-d**). The presence of TiO_2 is known to be beneficial for the deposition of PCN since the surface OH groups at titania surface act as a catalyst for the conversion of urea decomposition products to PCN [15, 33, 60, 61]. The shape of the nickel oxide particles was not affected by the deposition of TiO_2 (**Fig. 1e** and **g;** see also SEM analyses of NiO_x-TiO_2 at higher magnification in **Supporting Information**, **Fig. S4**), indicating that the TiO_2 layer is presumably very thin (< few nm). The slight increase of the particle average size to around 135 nm after the deposition of PCN is attributed to the PCN coating of the NiO_x particles.

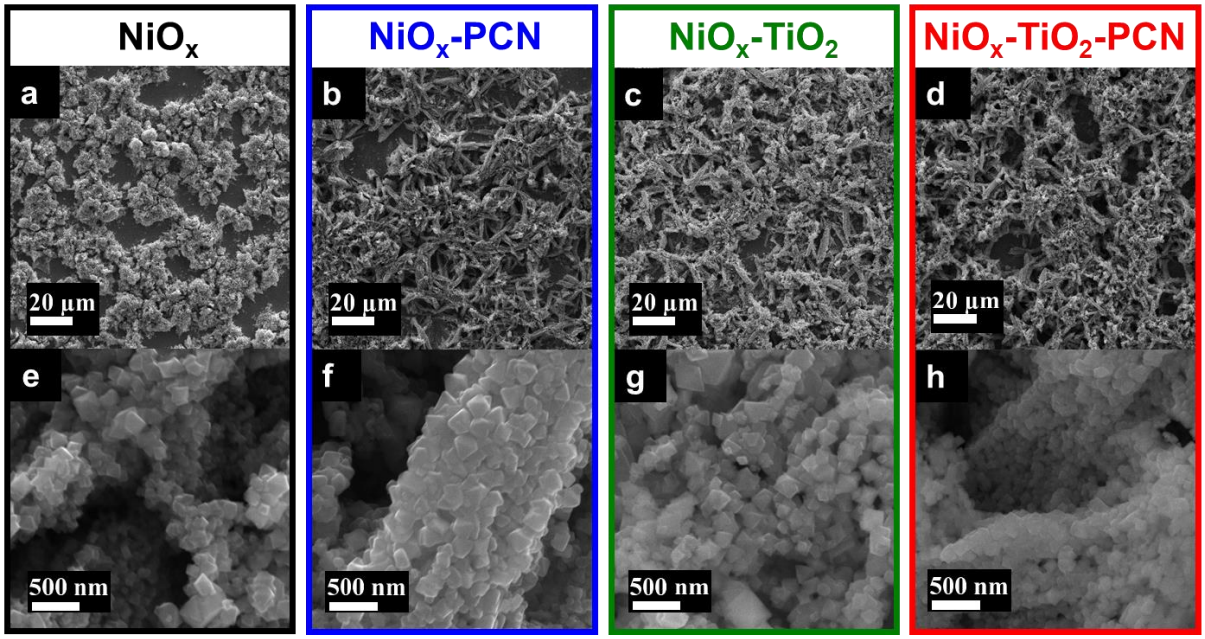

Fig. 1: Morphology of photocathodes. SEM images of NiO_x (a,e), NiO_x-PCN (b,f), NiO_x-TiO_2 (c,g), and NiO_x-TiO_2-PCN (d,h).

All four photoelectrodes exhibit very similar XRD patterns characteristic of a NiO cubic structure (see **Supporting Information, Fig. S1**). The lack of diffraction peaks characteristic of TiO_2 or PCN indicates that the amount of these components is low and/or that their structure is dominated by the amorphous phase. However, the presence of TiO_2 and PCN components was confirmed by EDS (see **Supporting Information, Tabs. S1** and **S2** and **Figs. S2** and **S3**) and FTIR measurements (see **Supporting Information, Fig. S9**). The cross-sectional SEM analysis at different magnifications (see **Supporting Information, Fig. S5**) shows that the multicomponent hybrid NiO_x-TiO_2-PCN photocathode has a thickness of ~ 15 µm and contacts

intimately with the FTO layer. The corresponding cross-section EDS elemental mapping images show that both TiO_2 and PCN are distributed along the whole thickness of the NiO_x porous film (see **Supporting Information, Fig. S5d** and **e**). Importantly, the fact that the regions of higher PCN and TiO_2 contents practically overlap confirms that the presence of TiO_2 has a beneficial effect on the chemical deposition of PCN. Top-view EDS elemental mapping images reveal a homogeneous distribution of Ni, Ti, C, N, and O in the NiO_x-TiO_2-PCN photocathode (see **Supporting Information, Fig. S6**). Notably, the thickness of the NiO_x-TiO_2 photocathode (~14 µm) is comparable to that of the NiO_x-TiO_2-PCN photocathode and the elemental distribution of Ni and Ti is highly homogeneous (see **Supporting Information, Fig. S7** and **S8**). All these results confirm that the photocathode thickness is governed by the porous NiO_x scaffold covered by a very thin TiO_2 layer that represents a suitable substrate for the chemical vapor deposition of a thin layer of PCN.

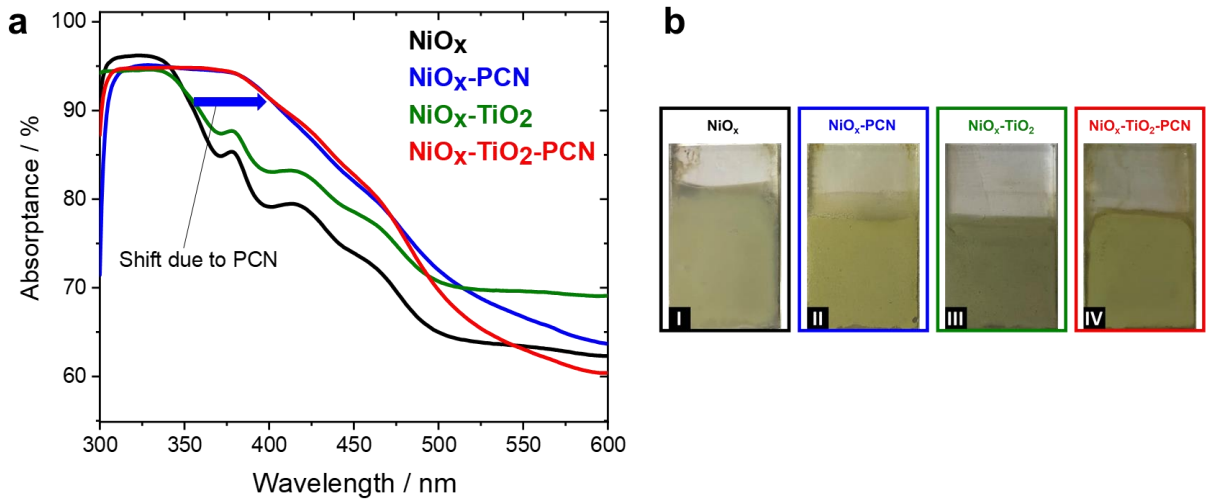

Fig. 2: Optical properties. (a) UV-Vis electronic absorption spectra of the NiO_x-containing photoelectrodes. (b) Optical images of the four electrodes, i) NiO_x, ii) NiO_x-PCN, iii) NiO_x-TiO_2 and iv) NiO_x-TiO_2-PCN. For the determination of bandgap using the Tauc formalism, see **Supporting information, Fig. S10**.

The electronic absorption spectra of all four photocathodes are shown in **Fig. 2**. For photocathodes without PCN, the fundamental absorption edge is below 350 nm (black and green curve), while the deposition of PCN clearly leads to increased absorption in the visible range (blue and red curves), which is evidenced by the yellowish color of these electrodes (**Fig. 2b**). This effect is similar to what is known for anatase TiO_2 (bandgap of 3.2 eV), where the deposition of PCN (bandgap of 2.7–2.9 eV) shifts the absorption edge to the visible. In order to determine the bandgap energies using the Tauc formalism, diffuse reflectance spectra of powders scratched off the electrodes were recorded (see **Supporting information, Fig. S10)**.

The optical bandgaps of NiO_x and NiO_x-TiO_2 materials were determined to be 3.3 eV, while the materials obtained after PCN deposition (NiO_x-PCN and NiO_x-TiO_2-PCN) exhibited a bandgap of 2.7 eV, which is in line with the typical optical absorption edge of PCN [62].

Next, we turn to studies of photoinduced changes in charge distribution at the surface of our photocathodes using surface photovoltage (SPV) spectroscopy [63]. In our SPV experiments, the contact potential difference (CPD), equivalent to the difference between the work functions of the sample and a gold reference probe, is measured under ambient conditions using the Kelvin probe technique. Surface photovoltage (SPV) is defined as the light-induced change of the CPD measured at the surface of a photoactive material. The sign of the SPV (*i.e.*, ΔCPD) signal, therefore, reflects the overall light-induced redistribution of charges between the surface and the bulk of the sample, which in turn affects the work function, and can give insights into the charge separation at illuminated photoactive materials [63]. Interestingly, the SPV measurements of our photocathodes show that only in the presence of PCN significant surface photovoltages are generated, whereas in PCN-free samples the SPV signal is negligible (**Fig. 3)**. The PCN layer strongly affects the change of the contact potential difference under irradiation with chopped monochromatic light down to 500 nm, in accord with the optical absorption spectra of these photoelectrodes (**Fig. 2**). Notably, the light-induced change of the CPD is *positive* for all PCN-containing samples at all wavelengths. The positive change of the CPD indicates an increase of the work function of the sample upon irradiation. It can be understood as a result of the change of the surface dipole by net separation of photoexcited electrons towards the PCN surface and of holes towards the bulk in the direction of the NiO_x hole-collecting scaffold. Three points are noteworthy in this context. Firstly, this behavior appears promising in view of operating our photoelectrodes as photocathodes capable of inducing reduction reactions in the electrolyte. Secondly, the magnitude of the SPV over the investigated wavelength range is higher for NiO_x-TiO_2-PCN than for the NiO_x-PCN material, which might indicate that the spatial charge separation is even more effective in the PCN sample with a TiO_2 interlayer. This is somewhat counterintuitive since TiO_2 is an *n*-type semiconductor and one would expect that it can effectively extract electrons from PCN, diminishing thus the SPV values. We hypothesize that, since the TiO_2 layer is rather thin, it can be easily penetrated by holes photogenerated in PCN, as in the case of so-called "leaky" TiO_2 layers used as passivating layers at silicon photoanodes [64, 65]. Thirdly, we point out that the SPV signal at PCN-containing samples is increasing continuously during irradiation, followed again by a continuous decrease after switching off the light. This relatively slow kinetics of CPD changes

is indicative of continuous accumulation and discharge of electrons in PCN, which has been observed for various types of PCN materials [30, 46, 66].

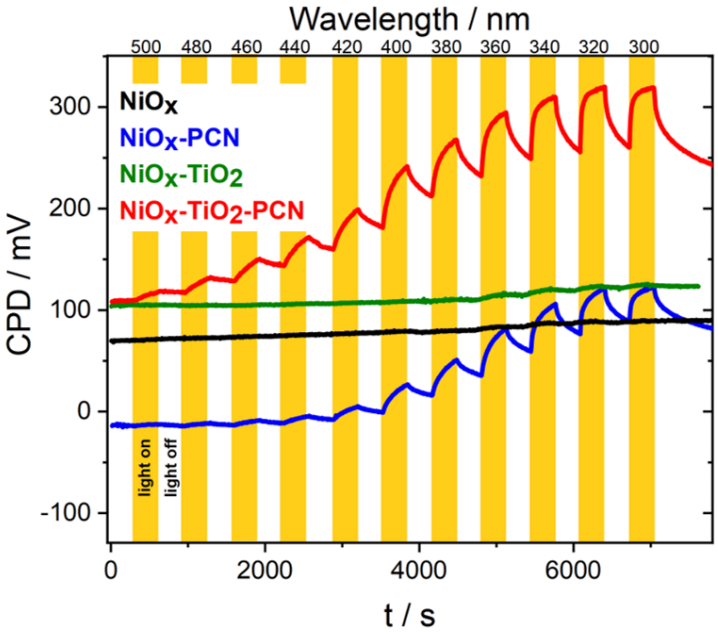

Fig. 3: **Surface photovoltage measurements.** Contact potential difference changes are recorded upon intermittent monochromatic light irradiation (320 s / 60 data points in the dark, 320 s / 60 data points under illumination) at different wavelengths under ambient conditions (in the air).

To investigate the charge separation and accumulation properties of all photocathodes also in the *electrolyte*, the open-circuit photopotential (OCP) for all electrodes was recorded at different wavelengths. In general, the light-induced change of the open-circuit potential reflects the change of the Fermi level of the FTO electrode upon illumination, whereby the Fermi level of FTO is expected to align with the *quasi*-Fermi level of holes in the *p*-type NiO_x scaffold. The differential OCP values, *i.e.* the difference between the OCP in the dark and under light, are shown in **Fig. 4**. Similar to the SPV measurements, the PCN-containing photocathodes show a significantly higher OCP response over a broad wavelength range, as compared to electrodes without PCN. For the NiO_x-PCN electrode under irradiation, the holes photogenerated in the PCN layer are preferentially transported to the underlying NiO_x and finally to the FTO glass, resulting in a *positive* (differential) OCP response. The presence or absence of oxygen in the solution had no significant effect on the observed OCP changes (see **Supporting Information**, **Fig. S11**). Interestingly, and again similar to the SPV measurements above, the TiO_2 interlayer between NiO_x and PCN significantly enhances the photopotentials at all wavelengths. To understand this effect, we assume, apart from the "leaky" nature of TiO_2 invoked already above, that a *p/n* junction formed between *p*-type NiO_x and *n*-type TiO_2 can enhance the charge separation and increase the observed photopotentials [67, 68].

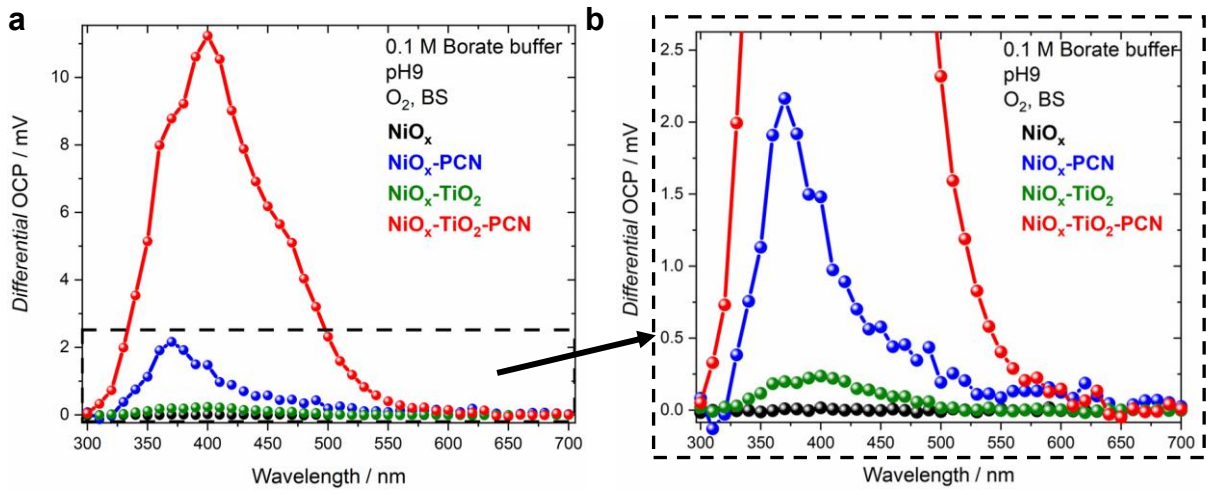

Fig. 4: **Measurements of *differential* open-circuit photopotential (OCP).** Differential OCP at different wavelengths was recorded for all photocathodes in borate buffer (0.1 M, pH 9) and irradiation was performed from the backside (through FTO). After stabilizing the system for over 10 min, the light was turned on and off every 5 s. The wavelengths were changed from 300 to 700 nm in 10 nm steps (a). The low OCP range is zoomed in (b).

All photocathode architectures were further characterized using potential-dependent photocurrent measurements under chopped simulated solar light. The cathodic scan of the NiO_x electrode (black curve, **Fig. 5**) shows two peaks. The peak at around 1.22 V *vs*. RHE correlates well with the Ni^{4+}/Ni^{3+} reduction potential, and the one at around 0.81 V *vs*. RHE is attributed to the Ni^{3+}/Ni^{2+} reduction [59, 69, 70]. The linear sweep voltammetry under intermittent illumination shows low photocurrents but a high dark current over the recorded potential range. Also for the NiO_x-TiO_2 electrode, a dark current can be observed that is relatively high, yet slightly lower than for bare NiO_x. It indicates that both NiO_x and NiO_x-TiO_2 electrodes can undergo a partial electrochemical reduction in this potential range (see also data recorded in the dark, **Supporting Information**, **Fig. S12**), and the TiO_2 layer does not completely passivate the NiO_x scaffold. On the other hand, the photocathodes comprising PCN, shown in red and blue (**Fig. 5**, compare also data recorded in the dark, **Supporting Information**, **Fig. S12**), exhibit negligible dark currents. This indicates that the NiO_x layer is nearly completely passivated after the deposition of PCN, and any electrochemical processes at these electrodes in the dark (without illumination) are inhibited in the studied potential range. A comparison of the photocurrents at +0.25 V *vs*. RHE shows that the NiO_x-TiO_2 exhibits the highest photocurrents (ca. –54 µA cm^{-2}), whereas the bare NiO_x electrode shows the lowest value (ca. –6 µA cm^{-2}). This result again corroborates the positive effect of the TiO_2 interlayer (*n*-type) on effective electron extraction from the *p*-type NiO_x scaffold due to the formation of a *p/n* junction [67, 68]. Notably, the deposition of PCN enhances slightly the photocurrents at NiO_x

(ca. –9 µA cm^{-2} for NiO_x-PCN) but diminishes them at NiO_x-TiO_2 (ca. –20 µA cm^{-2} for NiO_x-TiO_2-PCN). These results suggest an ambivalent role of PCN in our photocathodes. On the one hand, the PCN layer exerts a beneficial effect due to enhanced light harvesting and catalysis of O_2 reduction to H_2O_2 (see below). On the other hand, the effective passivation of the photocathodes by PCN also clearly leads to a partial decrease of photocurrents, as exemplified by the diminished photocurrents at NiO_x-TiO_2-PCN compared with NiO_x-TiO_2. Long-term photocurrent measurements have shown that the photocurrents are stable for at least four hours under 1 sun illumination (**Supporting Information**, **Fig. S13**).

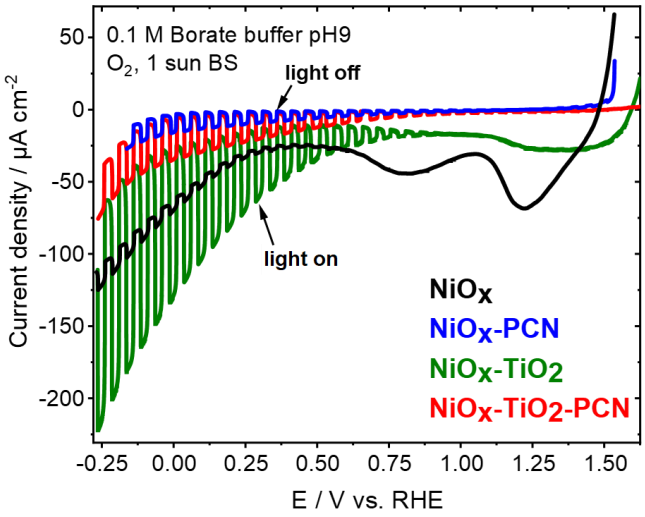

Fig. 5: **Photocurrent measurements.** Linear-sweep voltammetry (LSV) curves recorded in borate buffer (0.1 M, pH 9) under simulated solar light irradiation (scanned in cathodic direction with a sweep-rate of 5 mV s^{-1}.)

Further insights into the photoactivity of various photocathode architectures can be drawn from the measurements of the external quantum efficiencies. **Figure 6** shows the measurements of incident photon-to-current efficiencies (IPCE) of all photocathodes recorded in the range from 300 nm to 600 nm by illuminating the electrodes either from the backside (**Fig. 6a**) or from the frontside, *i.e.* through the electrolyte (**Fig. 6b**). As expected, the bare NiO_x electrode (bandgap of 3.3 eV ~ 376 nm) shows photocurrents in the UV range only. The deposition of the PCN layer results in a shift of the photoactivity to the visible range, which is in line with the optical, SPV and OCP measurements discussed above. We note that the highest IPCE values at NiO_x-TiO_2-PCN photocathodes (ca. 1.0%) are comparable to the highest IPCE values (ca. 1.5%) for the porphyrin-sensitized NiO photocathode reported by Mayer *et al.* [50].

The most surprising observation is the fact that the NiO_x-TiO_2 photocathode not only exhibits the highest IPCE values, which can be well conceived in terms of *p/n* junction formation, but exhibits a significant photoresponse even in the *visible* range (down to 550 nm). The latter

observation is rather puzzling given the fact that both NiO_x (bandgap of 3.3 eV) and TiO_2 (bandgap of 3.2 eV) have the fundamental absorption edge in the UV range. The most plausible explanation is that a significant density of intra-gap states is formed in TiO_2 after heating in the presence of NiO_x. Indeed, X-ray photoelectron spectroscopy (XPS) of NiO_x-TiO_2 revealed a significant amount of Ti^{3+} and of Ti^{4+} species with the binding energy shifted due to structural disorder-induced effects (see **Fig. S14** in the **Supporting Information**). The Ti^{3+} 3d states are known to lie energetically below the conduction band edge of TiO_2 [54]. Such occupied intra-gap states do not shift completely the fundamental absorption edge, but make themselves apparent as an absorption shoulder (Urbach tail) below the fundamental absorption edge (see **Fig. 2** and **Fig. S10** in the **Supporting Information**), and provide thus a plausible explanation for the significant sub-bandgap photocurrent response of the NiO_x-TiO_2 photocathode. Moreover, we hypothesize that, given the low thickness of the TiO_2 layer, the presence of these intra-gap states would further facilitate the "leaky" nature of the TiO_2 layer with respect to the transport of holes, as discussed above.

We now turn our attention to the differences in photoaction spectra between the backside (**Fig. 6a**) and frontside (**Fig. 6b**) illumination. The differences are subtle and complex. For all photocathode architectures except the NiO_x-TiO_2 electrode, the backside irradiation yields higher IPCE values at wavelengths above 350 nm. This is an expected behavior for porous photocathodes since for the backside irradiation the electrons and holes are generated closer to the FTO, and therefore the transport pathway for the holes is relatively short, whereby the electron transport is not a limiting factor, as the electrons are expected to readily react with electron acceptors in the solution that penetrates the whole volume of the porous electrode. In the case of the frontside irradiation, where most of the charges are generated in the vicinity of the electrode/electrolyte interface, the hole transport is typically the limiting factor in porous photocathodes because of the longer pathway for the holes to the FTO across the photoelectrode. Notably, at very low irradiation wavelengths (below 340 nm), the IPCE values are higher under the frontside illumination than under the backside illumination. We assume that this behavior, which is contradictory to the situation at longer wavelengths, is partly resulting from the parasitic UV light absorption by the FTO under backside illumination, but it also suggests that the photoresponse under high-energy UV irradiation is dominated by the NiO_x or NiO_x-TiO_2 scaffold. At the same time, since at very short wavelengths under the frontside illumination practically all charges are generated close to the electrode/electrolyte interface, the relatively high IPCE values in this range suggest that the intrinsic hole transport through the NiO_x layer is very efficient. This conclusion is also supported by the results obtained for the

NiO_x-TiO_2 electrode (green), which exhibits very high IPCE values independently of the illumination side. Hence, the very low IPCE values at PCN-modified photocathodes under frontside illumination in the visible range suggest that i) most of the photons in the visible range are harvested by PCN, and ii) that the hole injection from PCN into the NiO_x scaffold (either directly or through the TiO_2 interlayer) is the limiting process in photocurrent generation.

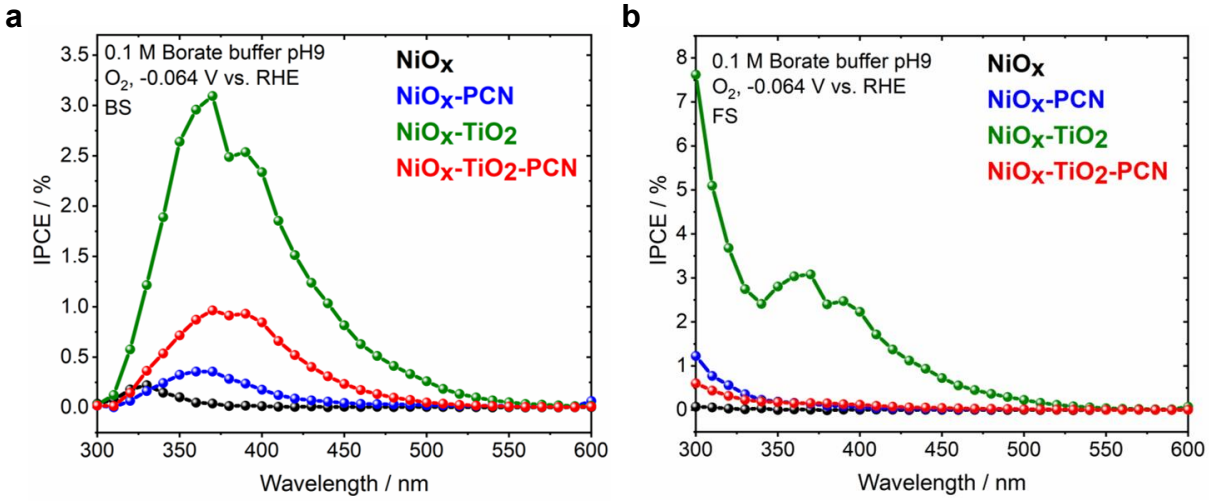

Fig. 6: **External quantum efficiencies**. IPCE spectra of the four photocathodes irradiated from the backside (a) and from frontside (b) recorded at –0.064 V *vs*. RHE in borate buffer (0.1 M, pH 9).

As the photocurrents at all photocathodes dropped significantly in the *absence* of dioxygen, it is clear that dioxygen dissolved in the solution acts as the main scavenger of photogenerated electrons. However, the key question to be addressed was whether H_2O_2 can be detected as a product of the photoelectrocatalytic conversion. Since the molar concentrations of H_2O_2 accumulated in our cells were below the detection limit of the conventional colorimetric H_2O_2 determination using a reaction with titanium peroxo-complex, we measured the H_2O_2 evolution *in-situ* using amperometric microsensors [55-57]. To this end, we used H_2O_2 microelectrodes (diameter of 25 μm) modified with Prussian blue (PB), as an effective electrocatalyst for H_2O_2 reduction, positioned approx. 50 μm above the photocathode surface as schematically shown in **Fig. 7**. At the PCN-modified photocathodes, monochromatic visible light (LED 420 nm) illumination caused an immediate current response at the PB-modified microelectrode, as exemplarily shown in the **Supporting Information**, **Fig. S15**. Importantly, no H_2O_2 was detected at PCN-free NiO_x and NiO_x-TiO_2 photoelectrodes (**Supporting Information**, **Fig. S15a** and **c**). The presence of PCN in the photocathode is therefore crucial in order to observe H_2O_2 as a product. Based on the Faraday's law, the total amount of H_2O_2 was determined to be 0.32 ± 0.08 pmol (n = 3) and 0.030 ± 0.007 pmol (n = 3) for the NiO_x-TiO_2-PCN and NiO_x-

PCN photocathodes, respectively (**Fig. 7**). As expected, no H_2O_2 was detected for PCN-containing photocathodes in the absence of dioxygen (**Supporting Information**, **Fig. S15e**).

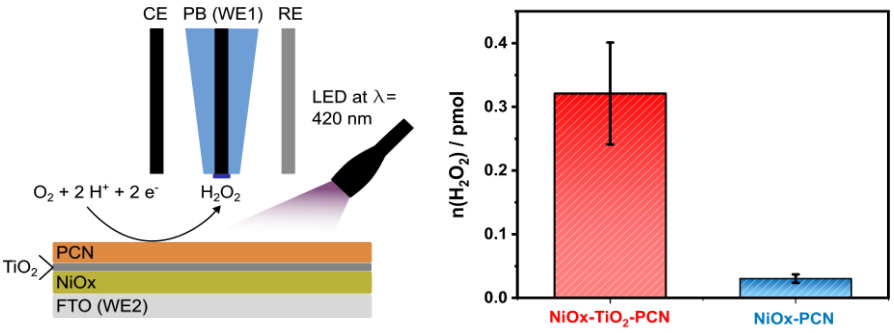

Fig. 7: *In-situ* H_2O_2 detection using a microsensor. (a) Scheme of the experimental setup. The PB-modified microelectrode (25 µm diameter) was positioned at a distance of 50 µm to the photocathode surface, the probed photocathode area was approximately 0.2 mm^2. The photocathodes were illuminated with monochromatic light (420 nm LED) for 10 min in a 1.5 mL phosphate buffer solution (50 mM, pH 7). The photocathodes were biased at –0.18 V *vs*. RHE, whereas the electrode potential of the sensor was set to +0.57 V *vs*. RHE. (b) A bar diagram of H_2O_2 amount determined during 10 min illumination of the NiO_x-TiO_2-PCN and NiO_x-PCN photocathodes (error bars reflect three repetitive measurements and are constructed as ±σ; σ = standard deviation). No H_2O_2 was detected at PCN-free NiO_x and NiO_x-TiO_2 photoelectrodes, and no H_2O_2 was detected for PCN-containing photocathodes in the absence of dioxygen.

These results demonstrate that PCN-containing photocathodes are capable of visible light-driven reduction of O_2 to H_2O_2, whereby the photocathode architecture comprising the TiO_2 interlayer exhibits the best performance both in terms of photocurrent and the amount of H_2O_2 formed. A simplified energy scheme depicting a possible mechanism of H_2O_2 formation at NiO_x-TiO_2-PCN photocathodes under visible light irradiation is shown in **Fig. 8**. As discussed above, Ti^{3+}-related intra-gap states are formed in TiO_2 interfaced with NiO_x. As the TiO_2 layer is very thin, these intra-gap states are also assumed to facilitate the hole transport across the TiO_2 film to the NiO_x hole-collecting scaffold. Please note that at least two different mechanisms of H_2O_2 formation are thermodynamically feasible. The two-electron reduction pathway, typically postulated for PCN materials in presence of additional electron donors [18, 44], has a larger thermodynamic driving force (1.4 V downhill) than a one-electron reduction to superoxide anion radical (0.9 V downhill), followed by disproportionation to H_2O_2 upon protonation of the superoxide anion radical: $O_2^{\bullet-} + H^+ \rightarrow HO_2^{\bullet}$, $2\,HO_2^{\bullet} \rightarrow H_2O_2 + O_2$ [50, 71]. In this context, we assume that the accumulation of electrons in the PCN layer observed in our SPV measurements (**Fig. 3**) might be beneficial for facilitating the two-electron reduction pathway. However, as for now, the question of the precise mechanism of H_2O_2 formation in our

system cannot be settled, as this will depend on a complex interplay between thermodynamic and kinetic factors and must be addressed by more detailed mechanistic studies.

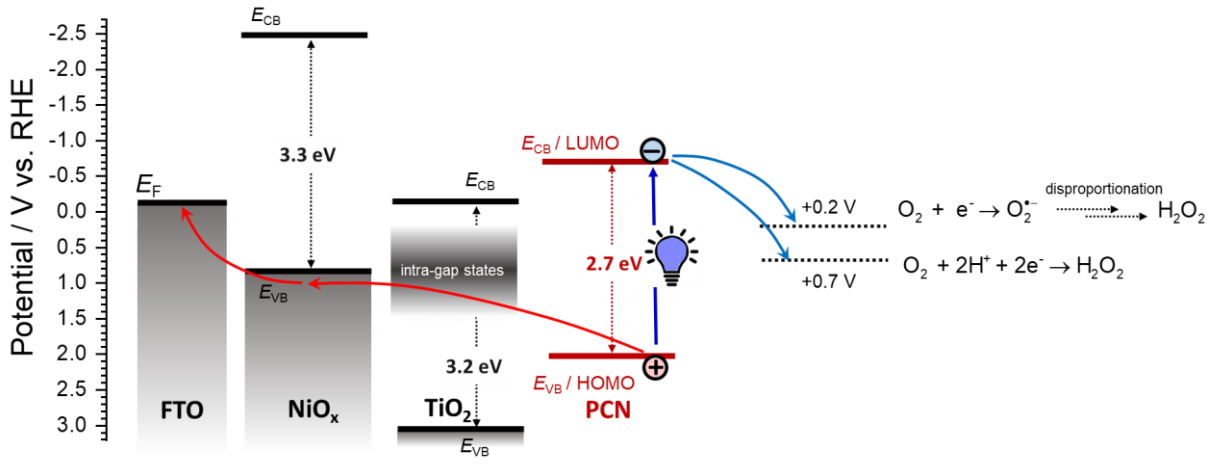

Fig. 8: A simplified energy scheme for H_2O_2 production at NiO_x-TiO_2-PCN photocathode. The approximate position of the valence band edge of NiO_x is taken from Ref. [50]; the positions of the band edges of TiO_2 and PCN are taken from Ref. [34]. All excitation processes apart from PCN and all possible recombination pathways are omitted for the sake of clarity. The presence of Ti^{3+} intra-gap states (see the text for details) is postulated to facilitate the hole transport through the TiO_2 layer. The formation of H_2O_2 is thermodynamically feasible both *via* a two-electron reduction pathway, as well as *via* a one-electron reduction to superoxide anion radical, followed by disproportionation to H_2O_2 and O_2 upon protonation of the superoxide anion radical [50, 71].

4. Conclusion

A multicomponent hybrid photocathode based on PCN that is capable of selective reduction of O_2 to H_2O_2 under visible light irradiation (420 nm LED) is reported for the first time. The optimized photocathode architecture comprises PCN deposited on a porous NiO_x film acting as a scaffold for effective extraction and collection of photogenerated holes, whereby a TiO_2 interlayer between NiO_x and PCN is found to exert a beneficial effect on the overall photoelectrocatalytic performance. The latter effect can be understood by assuming the formation of a *p/n* junction between the NiO_x and TiO_2 layers, as known from the literature [67, 68]. However, our photocurrent and XPS measurements also suggest that this is associated with the generation of intra-gap states that provide an explanation for the significant visible light photocurrent response of NiO_x-TiO_2 photoelectrodes and render the TiO_2 layer effectively "leaky" with respect to the transport of holes. Importantly, most of the studies on photocatalytic H_2O_2 production using PCN-based photocatalysts reported so far have been carried out in the presence of additional (sacrificial) electron donors such as aliphatic or aromatic alcohols. The fact that our PCN-based photocathodes catalyze the light-driven reduction of O_2 to H_2O_2 in the

absence of any additional electron donor confirms unambiguously that PCN materials are *inherently* photocatalytically active in H_2O_2 production. This significant finding thus paves the way for the development of further PCN-based photocathodes in which PCN could be coupled to more effective light absorbers in order to increase the overall performance. These efforts could eventually culminate in the construction of complete tandem devices comprising well-matched photocathodes and photoanodes, which would allow for bias-free operation in the light-driven selective synthesis of high-value commodity chemicals [72, 73].

Acknowledgments

This work was funded by the Deutsche Forschungsgemeinschaft (DFG – Projektnummer BE 5102/5-1, JA 1072/27-1, and 364549901– TRR 234 CataLight [Projects A5, B6, B10, C4] and by the National Science Centre, Poland (Solar-Driven Chemistry, 2019/01/Y/ST5/00027). The authors also acknowledge support by the state of Baden-Württemberg and the DFG through grant no. INST 40/574-1 FUGG

References

[1] X. Wang, K. Maeda, A. Thomas, K. Takanabe, G. Xin, J.M. Carlsson, K. Domen, M. Antonietti, Nat. Mater., 8 (2009) 76-80. 10.1038/nmat2317

[2] F.K. Kessler, Y. Zheng, D. Schwarz, C. Merschjann, W. Schnick, X. Wang, M.J. Bojdys, Nat. Mater. Rev., 2 (2017) 17030. 10.1038/natrevmats.2017.30

[3] A. Kubacka, U. Caudillo-Flores, I. Barba-Nieto, M. Fernández-García, Applied Catalysis A: General, 610 (2021) 117966. https://doi.org/10.1016/j.apcata.2020.117966

[4] V.W.-h. Lau, B.V. Lotsch, Adv. Energy. Mater., 12 (2022) 2101078. https://doi.org/10.1002/aenm.202101078

[5] D.J. Martin, K. Qiu, S.A. Shevlin, A.D. Handoko, X. Chen, Z. Guo, J. Tang, Angew. Chem. Int. ed., 53 (2014) 9240-9245. 10.1002/anie.201403375

[6] D.J. Martin, P.J.T. Reardon, S.J.A. Moniz, J. Tang, J. Am. Chem. Soc., 136 (2014) 12568-12571. 10.1021/ja506386e

[7] C.A. Caputo, L. Wang, R. Beranek, E. Reisner, Chem. Sci., 6 (2015) 5690-5694. 10.1039/c5sc02017d

[8] A. Rajagopal, E. Akbarzadeh, C.Y. Li, D. Mitoraj, I. Krivtsov, C. Adler, T. Diemant, J. Biskupek, U. Kaiser, C. Im, M. Heiland, T. Jacob, C. Streb, B. Dietzek, R. Beranek, Sustain. Energy Fuels, 4 (2020) 6085-6095. 10.1039/d0se01366h

[9] D. Mitoraj, I. Krivtsov, C. Li, A. Rajagopal, C. Im, C. Adler, K. Köble, O. Khainakova, J. Hniopek, C. Neumann, A. Turchanin, I. da Silva, M. Schmitt, R. Leiter, T. Lehnert, J. Popp, U. Kaiser, T. Jacob, C. Streb, B. Dietzek, R. Beranek, Chem. Eur. J., 27 (2021) 17188-17202. https://doi.org/10.1002/chem.202102945

[10] Y. Zhang, D. Liu, J. Shi, P. Chen, S. Zong, C. Cheng, K. Chen, Y. Chen, L. Ma, Applied Catalysis A: General, 643 (2022) 118746. https://doi.org/10.1016/j.apcata.2022.118746

[11] M. Bledowski, L. Wang, S. Neubert, D. Mitoraj, R. Beranek, J. Phys. Chem. C, 118 (2014) 18951-18961. 10.1021/jp506434a

[12] R. Gong, D. Mitoraj, D. Gao, M. Mundszinger, D. Sorsche, U. Kaiser, C. Streb, R. Beranek, S. Rau, Adv. Sustainable Syst., 6 (2022) 2100473. https://doi.org/10.1002/adsu.202100473

[13] G. Gao, Y. Jiao, E.R. Waclawik, A. Du, J. Am. Chem. Soc., 138 (2016) 6292-6297. 10.1021/jacs.6b02692

[14] G. Zhao, H. Pang, G. Liu, P. Li, H. Liu, H. Zhang, L. Shi, J. Ye, Appl. Catal. B: Environ., 200 (2017) 141-149. https://doi.org/10.1016/j.apcatb.2016.06.074

[15] D. Mitoraj, H. Kisch, Angew. Chem. Int. ed., 47 (2008) 9975-9978. https://doi.org/10.1002/anie.200800304

[16] Y. Guo, S. Huang, Y. Guo, Z. Ye, J. Nan, Q. Zhou, Y. Zhu, Appl. Catal. B: Environ., 312 (2022) 121388. https://doi.org/10.1016/j.apcatb.2022.121388

[17] C. Yin, Y. Liu, X. Kang, X. Li, Applied Catalysis A: General, 636 (2022) 118571. https://doi.org/10.1016/j.apcata.2022.118571

[18] Y. Shiraishi, S. Kanazawa, Y. Sugano, D. Tsukamoto, H. Sakamoto, S. Ichikawa, T. Hirai, ACS Catalysis, 4 (2014) 774-780. 10.1021/cs401208c

[19] A. Savateev, I. Ghosh, B. Konig, M. Antonietti, Angew. Chem. Int. Ed., 57 (2018) 15936-15947. 10.1002/anie.201802472

[20] I. Ghosh, J. Khamrai, A. Savateev, N. Shlapakov, M. Antonietti, B. Konig, Science, 365 (2019) 360-366. 10.1126/science.aaw3254

[21] I. Krivtsov, D. Mitoraj, C. Adler, M. Ilkaeva, M. Sardo, L. Mafra, C. Neumann, A. Turchanin, C. Li, B. Dietzek, R. Leiter, J. Biskupek, U. Kaiser, C. Im, B. Kirchhoff, T. Jacob, R. Beranek, Angew. Chem. Int. Ed., 59 (2020) 487-495. 10.1002/anie.201913331

[22] J. Schneider, D.W. Bahnemann, J. Phys. Chem. Lett., 4 (2013) 3479-3483. 10.1021/jz4018199

[23] F. Costantino, P.V. Kamat, ACS Energy Lett., 7 (2022) 242-246. 10.1021/acsenergylett.1c02487

[24] H. Ou, P. Yang, L. Lin, M. Anpo, X. Wang, Angew. Chem. Int. Ed., 56 (2017) 10905-10910.10.1002/anie.201705926

[25] F. Podjaski, J. Kroger, B.V. Lotsch, Adv. Mater., 30 (2018) 1705477. 10.1002/adma.201705477

[26] J. Qin, J. Barrio, G. Peng, J. Tzadikov, L. Abisdris, M. Volokh, M. Shalom, Nat. Commun., 11 (2020) 4701. 10.1038/s41467-020-18535-0

[27] N. Karjule, J. Barrio, L. Xing, M. Volokh, M. Shalom, Nano Lett., 20 (2020) 4618-4624. 10.1021/acs.nanolett.0c01484

[28] M. Shalom, S. Gimenez, F. Schipper, I. Herraiz-Cardona, J. Bisquert, M. Antonietti, Angew. Chem. Int. Ed., 53 (2014) 3654-3658. 10.1002/anie.201309415

[29] C. Adler, I. Krivtsov, D. Mitoraj, L. dos Santos-Gómez, S. García-Granda, C. Neumann, J. Kund, C. Kranz, B. Mizaikoff, A. Turchanin, R. Beranek, ChemSusChem, 14 (2021). https://doi.org/10.1002/cssc.202100313

[30] C. Adler, S. Selim, I. Krivtsov, C. Li, D. Mitoraj, B. Dietzek, J.R. Durrant, R. Beranek, Adv. Funct. Mater., 31 (2021) 2105369. https://doi.org/10.1002/adfm.202105369

[31] M. Bledowski, L. Wang, A. Ramakrishnan, R. Beranek, J. Mater. Res., 28 (2013) 411-417. doi:10.1557/jmr.2012.297

[32] M. Bledowski, L. Wang, A. Ramakrishnan, A. Bétard, O.V. Khavryuchenko, R. Beranek, ChemPhysChem, 13 (2012) 3018-3024. 10.1002/cphc.201200071

[33] M. Bledowski, L. Wang, A. Ramakrishnan, O.V. Khavryuchenko, V.D. Khavryuchenko, P.C. Ricci, J. Strunk, T. Cremer, C. Kolbeck, R. Beranek, Phys. Chem. Chem. Phys., 13 (2011) 21511-21519. 10.1039/c1cp22861g

[34] L. Wang, D. Mitoraj, S. Turner, O.V. Khavryuchenko, T. Jacob, R.K. Hocking, R. Beranek, ACS Catal., 7 (2017) 4759-4767. 10.1021/acscatal.7b01466

[35] P. Longchin, D. Mitoraj, O.M. Reyes, C. Adler, N. Wetchakun, R. Beranek, J. Phys. Energy, 2 (2020) 044001. 10.1088/2515-7655/abaec9

[36] C. Pulignani, C.A. Mesa, S.A.J. Hillman, T. Uekert, S. Giménez, J.R. Durrant, E. Reisner, Angew. Chem. Int. ed., 61 (2022) e202211587. https://doi.org/10.1002/anie.202211587

[37] Q. Ruan, T. Miao, H. Wang, J. Tang, J. Am. Chem. Soc., 142 (2020) 2795-2802. 10.1021/jacs.9b10476

[38] Y. Zhang, Z. Schnepp, J. Cao, S. Ouyang, Y. Li, J. Ye, S. Liu, Sci. Rep., 3 (2013) 2163. 10.1038/srep02163

[39] F. Yang, M. Lublow, S. Orthmann, C. Merschjann, T. Tyborski, M. Rusu, S. Kubala, A. Thomas, R. Arrigo, M. Hävecker, T. Schedel-Niedrig, ChemSusChem, 5 (2012) 1227-1232. https://doi.org/10.1002/cssc.201100691

[40] H. Yu, H. Cohen, R. Neumann, Chem. Eur. J., 27 (2021) 13513-13517. https://doi.org/10.1002/chem.202101820

[41] Y. Dong, Y. Chen, P. Jiang, G. Wang, X. Wu, R. Wu, RSC Adv., 6 (2016) 7465-7473. 10.1039/C5RA23265A

[42] Z. Wang, G. Zou, C. Feng, Y. Ma, X. Wang, Y. Bi, RSC Adv., 6 (2016) 83350-83355. 10.1039/C6RA18999G

[43] H. Hou, X. Zeng, X. Zhang, Angew. Chem. Int. ed., 59 (2020) 17356-17376. https://doi.org/10.1002/anie.201911609

[44] Y. Shiraishi, S. Kanazawa, Y. Kofuji, H. Sakamoto, S. Ichikawa, S. Tanaka, T. Hirai, Angew. Chem. Int. ed., 53 (2014) 13454-13459. 10.1002/anie.201407938

[45] P. Zhang, Y. Tong, Y. Liu, J.J.M. Vequizo, H. Sun, C. Yang, A. Yamakata, F. Fan, W. Lin, X. Wang, W. Choi, Angew. Chem. Int. ed., 59 (2020) 16209-16217. https://doi.org/10.1002/anie.202006747

[46] C. Li, E. Hofmeister, I. Krivtsov, D. Mitoraj, C. Adler, R. Beranek, B. Dietzek, ChemSusChem, 14 (2021) 1728-1736. https://doi.org/10.1002/cssc.202002921

[47] P. Sharma, T.J.A. Slater, M. Sharma, M. Bowker, C.R.A. Catlow, Chem. Mater., 34 (2022) 5511-5521. 10.1021/acs.chemmater.2c00528

[48] F. Su, S.C. Mathew, G. Lipner, X. Fu, M. Antonietti, S. Blechert, X. Wang, J. Am. Chem. Soc., 132 (2010) 16299-16301. 10.1021/ja102866p

[49] M. Jakešová, D.H. Apaydin, M. Sytnyk, K. Oppelt, W. Heiss, N.S. Sariciftci, E.D. Głowacki, Adv. Funct. Mater., 26 (2016) 5248-5254. https://doi.org/10.1002/adfm.201601946

[50] O. Jung, M.L. Pegis, Z. Wang, G. Banerjee, C.T. Nemes, W.L. Hoffeditz, J.T. Hupp, C.A. Schmuttenmaer, G.W. Brudvig, J.M. Mayer, J. Am. Chem. Soc., 140 (2018) 4079-4084. 10.1021/jacs.8b00015

[51] L. Li, E.A. Gibson, P. Qin, G. Boschloo, M. Gorlov, A. Hagfeldt, L. Sun, Adv. Mater., 22 (2010) 1759-1762. https://doi.org/10.1002/adma.200903151

[52] P. Makuła, M. Pacia, W. Macyk, J. Phys. Chem. Lett., 9 (2018) 6814-6817. 10.1021/acs.jpclett.8b02892

[53] M.C. Biesinger, B.P. Payne, A.P. Grosvenor, L.W.M. Lau, A.R. Gerson, R.S.C. Smart, Appl. Surf. Sci., 257 (2011) 2717-2730. https://doi.org/10.1016/j.apsusc.2010.10.051

[54] J. Saari, H. Ali-Löytty, M.M. Kauppinen, M. Hannula, R. Khan, K. Lahtonen, L. Palmolahti, A. Tukiainen, H. Grönbeck, N.V. Tkachenko, M. Valden, J. Phys. Chem. C, 126 (2022) 4542-4554. 10.1021/acs.jpcc.1c10919

[55] O.G. Voronin, A. Hartmann, C. Steinbach, A.A. Karyakin, A.R. Khokhlov, C. Kranz, Electrochem. Commun., 23 (2012) 102-105. https://doi.org/10.1016/j.elecom.2012.07.017

[56] M.A. Komkova, A. Holzinger, A. Hartmann, A.R. Khokhlov, C. Kranz, A.A. Karyakin, O.G. Voronin, Beilstein J. Nanotechnol., 4 (2013) 649-654. 10.3762/bjnano.4.72

[57] A. Hellmann, S. Daboss, F. Zink, C. Hartmann, P. Radermacher, C. Kranz, Electrochim. Acta, 353 (2020) 136458. https://doi.org/10.1016/j.electacta.2020.136458

[58] M. Bonomo, D. Dini, F. Decker, Front. Chem., 6 (2018). 10.3389/fchem.2018.00601

[59] C.J. Wood, G.H. Summers, C.A. Clark, N. Kaeffer, M. Braeutigam, L.R. Carbone, L. D'Amario, K. Fan, Y. Farré, S. Narbey, F. Oswald, L.A. Stevens, C.D.J. Parmenter, M.W. Fay, A. La Torre, C.E. Snape, B. Dietzek, D. Dini, L. Hammarström, Y. Pellegrin, F. Odobel, L. Sun, V. Artero, E.A. Gibson, Phys. Chem. Chem. Phys., 18 (2016) 10727-10738. 10.1039/C5CP05326A

[60] D. Mitoraj, H. Kisch, Chem.--Eur. J., 16 (2010) 261-269, S261/261-S261/265. 10.1002/chem.200901646

[61] R. Gong, D. Mitoraj, R. Leiter, M. Mundszinger, A.K. Mengele, I. Krivtsov, J. Biskupek, U. Kaiser, R. Beranek, S. Rau, Front. Chem., 9 (2021). 10.3389/fchem.2021.709903

[62] C. Im, B. Kirchhoff, I. Krivtsov, D. Mitoraj, R. Beranek, T. Jacob, Chem. Mater., (2023). 10.1021/acs.chemmater.2c02843

[63] L. Kronik, Y. Shapira, Surf. Sci. Rep., 37 (1999) 1-206. https://doi.org/10.1016/S0167-5729(99)00002-3

[64] S. Hu, M.R. Shaner, J.A. Beardslee, M. Lichterman, B.S. Brunschwig, N.S. Lewis, Science, 344 (2014) 1005-1009. 10.1126/science.1251428

[65] T. Moehl, J. Suh, L. Sévery, R. Wick-Joliat, S.D. Tilley, ACS Appl. Mater. Interfaces, 9 (2017) 43614-43622. 10.1021/acsami.7b12564

[66] W. Yang, R. Godin, H. Kasap, B. Moss, Y. Dong, S.A.J. Hillman, L. Steier, E. Reisner, J.R. Durrant, J. Am. Chem. Soc., 141 (2019) 11219-11229. 10.1021/jacs.9b04556

[67] J. Guo, W. Fu, H. Yang, Q. Yu, W. Zhao, X. Zhou, Y. Sui, J. Ding, Y. Li, S. Cheng, M. Li, J. Phys. D: Appl. Phys., 43 (2010) 245202. 10.1088/0022-3727/43/24/245202

[68] C. Shifu, Z. Sujuan, L. Wei, Z. Wei, J. Hazard. Mater., 155 (2008) 320-326. https://doi.org/10.1016/j.jhazmat.2007.11.063

[69] B.A. Nail, J.M. Fields, J. Zhao, J. Wang, M.J. Greaney, R.L. Brutchey, F.E. Osterloh, ACS Nano, 9 (2015) 5135-5142. 10.1021/acsnano.5b00435

[70] A.G. Marrani, V. Novelli, S. Sheehan, D.P. Dowling, D. Dini, ACS Appl. Mater. Interfaces, 6 (2014) 143-152. 10.1021/am403671h

[71] B.H.J. Bielski, A.O. Allen, J. Phys. Chem., 81 (1977) 1048-1050. 10.1021/j100526a005

[72] E. Reisner, Angew. Chem. Int. ed., 58 (2019) 3656-3657. 10.1002/anie.201814692

[73] R. Beranek, Angew. Chem. Int. ed., 58 (2019) 16724-16729. 10.1002/anie.201908654